Bergen Center for Computational Science

BCCS
TECHNICAL REPORT SERIES

Numerical study of particle encounters with an idealized coral reef with focus on grid resolutions and viscosities

Thiem, Ø., Berntsen, J., Selvikvåg, K., Fosså, J.H.

REPORT No. 24 **November 14, 2008**

Deliverance to Cordino.
Contract number 146526/420

UNIFOB
the University of Bergen research company

BERGEN, NORWAY

BCCS Technical Report Series is available at http://www.bccs.no/publications/

Requests for paper copies of this report can be sent to:

Bergen Center for Computational Science, Høyteknologisenteret,
Thormøhlensgate 55, N-5008 Bergen, Norway

Abstract

A two dimensional numerical non-hydrostatic study of a constant flow over an idealized reef has been performed and areas where passive particles enter close enough to the seabed for corals to catch them have been identified. Results for different horizontal and vertical viscosities, horizontal and vertical grid resolutions are presented in the report. The model result shows that for Reynolds number $\sim 10^5 - 10^6$ the majority of the particles enter close to the seabed at the side of the idealized reef that face the current. If food brought to the corals by the current is decisive for the coral growth and reef building, this research shows that in areas with predominantly homogeneous current direction, deep water coral reefs will grow into elongated shapes while in areas with varying current direction, circular shaped reefs will develop. This is in agreement with findings at the Norwegian shelf.

1 Introduction

The cold-water coral *Lophelia pertusa* (L., 1758) is found at the Norwegian shelf. The shape of the coral reefs varies, but in areas where the current direction is predominant from one direction elongated reefs with a living head and a dead tail is most common. In areas where the current direction varies more bell shaped reefs are found.

This study investigates numerically how particles are transported by the current and identifies where particles are most likely to enter the lower 0.25 m above seabed, which in this study will be defined as the benthic layer. A two dimensional version of a numerical ocean model has been used for the studies. The model is set up and run with numerous various grid resolutions and viscosities to identify the results sensitivity to these parameters. The results will found the basis for further numerical studies of coral distribution, location, and growth.

General information about the model is found in Section 2.1, and more specific details concerning the setup used in this study is found in Section 2.2. The numerical results from the model are found in Section 3, which is separated into parts containing increased horizontal (Section 3.1), vertical grid resolution (Section 3.2), and a part containing the sensitivity to the horizontal and vertical viscosities, bottom friction, and the hydrostatic approximation (Section 3.3). The discussion is found in Section 4.

2 Methods

2.1 The numerical model

The Bergen Ocean Model (BOM) has a terrain following vertical coordinate and equidistant grid in the horizontal. The advantage with a terrain following model is increased resolution close to the seabed. A two dimensional (2D) version of BOM with the coordinate system (x, σ, t), where x is the horizontal coordinate, σ the vertical coordinate, and t is the time, is used for the present studies. In the vertical, the standard σ-transformation, $\sigma = \frac{z-\eta}{H+\eta}$, is applied, where z is the vertical Cartesian coordinate, η the surface elevation, and H the bottom depth. The variables are discretized on a C-grid, and the model is thorough described in Berntsen [2000] and available from www.mi.uib.no/BOM/ .

The horizontal movement (advection) of momentum and density is done with a Total Variation Diminishing (TVD) scheme which have the advantage that it does not provide non-physical solutions. A superbee limiter described in Yang and Przekwas [1992] is applied in the present studies to avoid spurious oscillations in the solution where sharp variations in the fields are present. The standard second order POM method is applied to estimate the internal pressure gradients [Blumberg and Mellor, 1987, Mellor, 1996]. The model is mode split in a barotropic mode which is the fast moving signals connected to the surface, and a baroclinic mode which resolves the slower interior signals. Such a mode splitting save computational time since the full equations are solved more rare than the barotropic equations. The mode splitting method used in this study is similar to the splitting described in Berntsen et al. [1981] and Kowalik and Murty [1993].

Ocean models often use the hydrostatic approximation, which assume that the primary balance in the vertical is between the gravitational force and the vertical pressure gradient. However, this assumption is violated in the presence of steep topography, where other terms of the vertical momentum equation might be significant. The simulations in this work is therefore run non-hydrostatic. In BOM a time splitting technique is used, where the hydrostatic model first compute provisional velocities $\tilde{U}$ and $\tilde{W}$ in the x- and z-direction respectively. Based on the divergence of these provisional velocities, the non-hydrostatic pressure P_{NH} may be computed by inserting the expression for the non-hydrostatic velocity corrections into the equation of continuity [Kanarska and Maderich, 2003, Heggelund et al., 2004]. Due to the σ-transformation, additional terms appear in the momentum equation,

which complicates the computations considerably. An alternative method, that has been used in the present study, is to view the non-hydrostatic pressure directly as $P_{NH}(x, \sigma, t)$ or a pressure due to convergence or divergence in the σ-coordinate system [Berntsen and Furnes, 2005]. The non-hydrostatic pressure may as before be computed by inserting the expressions for non-hydrostatic velocity corrections into the equation of continuity. However, with the present approach the elliptic equation for the non-hydrostatic pressure get the same structure as the pressure equation in z-coordinate models, and this simplifies the computations considerably. The gradient of $P_{NH}(x, \sigma, t)$ is used in the final stages of a time step to adjust the velocity components to become divergence free.

The solution is moved (stepped) forward in time by predictor-corrector methods in BOM. The external time steps are performed with a predictor-corrector method where the leapfrog method is used as predictor and fully implicit method is used as the corrector [Haidvogel and Beckmann, 1999, Casulli, 1999]. The internal time steps are performed with a predictor-corrector method where the leapfrog method is used as predictor and the Adams-Moulton 2-step method is used as a corrector, see Heimsund and Berntsen [2004] for analysis of the stability of this pair.

The interface between the bottom and the water creates a boundary layer where momentum, vorticity and the energy in the system are removed. This interface generates a bottom boundary layer which is a region where the shear generates turbulence and the tangential flow component will have a logarithmic vertical profile [Haidvogel and Beckmann, 1999]. The height of the bottom boundary layer will depend on the local topographic features in the area, and the effect is parametrized through the bottom stress $\tau_b(x, t)$ specified by

$$\tau_b(x, t) = \rho_0 C_D \sqrt{{u_b}^2} u_b(x, t). \tag{1}$$

Here ρ_0 is the reference density, $u_b(x, t)$ is the velocity in the nearest bottom grid cell, in the x-direction. The drag coefficient C_D is given by

$$C_D = \max[0.0025, \frac{\kappa^2}{(ln(z_b/z_0))^2}], \tag{2}$$

where z_b is the distance of the nearest grid point to the bottom. The von Karman constant κ is 0.4 and the bottom roughness parameter is chosen to be z_0 = 0.0002 m, see Blumberg and Mellor [1987].

2.2 Model setup

The model domain is $l_x = 396.8$ m long with a maximum deep of $h_b = 300$ m. Approximately in the middle (at $x_m = 197.6$ m) a $h_m = 16$ m high and a $2r_m = 90$ m wide hill, mimicking a coral reef is located. The function used to create the reef is given by

$$H(x) = h_b + \frac{h_m}{2} \cos(\frac{\pi x}{r_m} + \pi) - \frac{h_m}{2}, \qquad x_m - r_m < x < x_m + r_m. \tag{3}$$

As Equation 3 shows, the shape of the reef is a cosine function ranging from minimum to minimum that sticks up from a flat bottom with a depth of h_b. It can be shown that the maximum slope of the reef will be approximately 0.56 and is located at $x_m \pm r_m/2.0$. In Equation 3, r_m is the radius of the reef and x is the horizontal grid coordinate. Reefs with approximately this height and length parameters can found on the Norwegian continental shelf. The mean height and length and also shape of four of the coral reefs in this area are used to compute the parameters needed for this idealized reef set up.

The grid resolution will decide what physics that can be resolved in the model. To investigate the sensitivity of the numerical results to variations in the horizontal and the vertical grid resolution several experiments are performed. An overview of the experiments and the results is given in Table 1. The grid resolution is equidistant in the horizontal. In

Exp 1-7 and 15-29 the 10 vertical grid cells closest to the bottom is equidistant with the values found in Table 1. The remaining layers are gradually coarser toward the surface. In Exp 8-14 the lower 12.8 m is distributed by layers of $min(\Delta z)$ given in Table 1 and the remaining layers are distributed by a function that are exponential getting coarser toward the surface. The number of vertical layers in these experiments are found in Table 1.

The model is run with homogeneous density. This is mainly due to the expectation that the water masses close to the bottom is well mixed on the continental shelf. This also allows us to exclude the effect of the stratification which can lead to a blocking effect and generation of a hydraulic jump at the rear of the reef.

The initial conditions interior in the model domain is a barotropic current which is computed as

$$u = u_0 * h_b/h_u \,, \tag{4}$$

where u_0 is the horizontal velocity forced at the boundary and h_u is the depth in u points in the domain. This choice of u will lead to a very short transient spin up phase, and only after a couple of time steps u and w will be adjusted to the flow.

To avoid wave reflection and allow flow in and out of the model domain two open boundaries at $x = 0.0$ m and $x = l_x$ are used. At the open boundaries 7 grid cells wide FRS zones are implemented [Engedahl, 1992]. On the inflowing boundary a horizontal barotropic constant velocity of $u_0 = 0.25\,\mathrm{ms}^{-1}$ is used to force the flow. The surface elevation (η) on the inflowing boundary is updated with respect to the model response to the flow. On the outflowing boundary the horizontal and vertical velocities, η, and depth averaged horizontal flow are updated with the same technique as η on the inflowing boundary.

Physics on scales less than some grid cells can not be resolved in numerical models. This physics are referred to sub grid scale processes, and energy from this physics need to be dealt with. This is done by choosing a level of viscosity and diffusivity to be included in the model. Viscosity and diffusivity is also introduced through the numerical schemes, and in Exp 1-14 and 27-29 only the numerical viscosity in the horizontal and molecular eddy viscosity in the vertical are used.

The bottom stress is given in Equation 1 where the drag coefficient is found in Equation 2. The bottom roughness parameter is chosen to be $z_0 = 0.005$ m. In Exp 21 the bottom stress is set to zero to investigate the influence the bottom stress have on the numerical results. All the experiments are run without rotation, but on this scale the effect from the rotation is negligible.

For the experiments 30 external (barotropic) time steps per internal (baroclinic) step is used. The horizontal Courant number is approximately 0.5 in the simulations.

2.3 The particle model

20 000 particles are randomly spread in the x-direction and between $h_b - 20$ m and $H(x) - h_c$ where $h_c = \frac{0.25}{cos\,\theta}$ m. Here θ is the slope angle, and the $cos\,\theta$ term accounts for that corals can reach perpendicular to the seabed in variable topography. In the study h_c will be called the lower benthic layer. The particles are passive tracers that will drift with the currents according to

$$\vec{x}_p^{\,n+1} = \vec{x}_p^{\,n} + \Delta t \vec{u}^{\,n}. \tag{5}$$

Here $\vec{x}_p^{\,n}$ is the location of a particle at time step n, Δt the time step size, and $\vec{u}^{\,n}$ the velocity of the water at the tracer location at time step n. A random step in the horizontal and vertical is implemented for the particles,

$$\vec{x}_p^{\,n+1} = \vec{x}_p^{\,n+1} + r \cdot \Delta t \vec{u}_{std}^{\,n}, \tag{6}$$

where r is a random number between zero and one, and $\vec{u}_{std}^{\,n}$ is the standard deviation of the velocity components at timestep n.

Particles that enter the lower benthic layer is taken out of the simulation and the location is marked so areas where particles enter into reach for the corals are identified. Areas with

a high hit rate indicate places where food is transported close to the seabed by the currents and therefore can be suitable locations for corals.

Periodic boundary conditions are used for the particles on the open boundaries. The periodic boundary conditions will allow the particles that imitate the food for the corals to be transported out of the region at one end and re-enter in the other end.

3 Results

The pathlines of some of the particles are shown in Figure 1. The figure shows that the flow reminds of potential flow, however, there is a slight asymmetry. From Figure 1 it can be seen that the particles will have a minimum perpendicular distance from the slope in the steepest part of the slope and the perpendicular distance changes most where the variation in topography is highest.

From Figure 2 it is possible to estimate the level of numerical viscosity from the simulations where the horizontal viscosity is set equal to zero. A crude estimate of the viscosity is $10^{-4} - 10^{-3}\,\mathrm{m^2 s^{-1}}$ which leads to a Reynolds Number $Re = u_0 \cdot 2r_m/\mu \sim 10^4 - 10^5$ (for $u_0 = 0.25$ and $L = 90$). This means that the flow is close to turbulent. It can be seen from Figure 1 that the flow is not turbulent and firmer study of the flow pattern show that the flow is laminar for this coral reef. The non dimensional height ($h_m/h_b \sim 5 \cdot 10^{-2}$) shows that the blocking effect is small for the simulations. If stratification is introduced, the blocking effect could be substantial leading to an increase in the velocities. This could lead to a increase in the Reynolds Number and a turbulent flow. The divergence for 2D (x, z) homogeneous fluid flow is given by

$$\frac{\partial u}{\partial x} + \frac{\partial w}{\partial z} = 0. \tag{7}$$

Equation 7 shows that when u is increasing, for instance due to conservation of volume when encountering an obstacle, there will be a positive vertical flow that decreases with distance from the obstacle and will have the maximum at the steepest part of the obstacle. This means that the streamlines will be compressed when facing an obstacle, see Kundu and Cohen [1990], and the distance between the bottom and the passive particles moving with the current will decrease. This is seen in the pathlines in Figure 1. When the flow passes over the obstacle and enters deeper water u will decrease and the vertical flow will be negative. The highest negative vertical velocity will be found in the steepest part of the down slope.

3.1 Sensitivity to horizontal grid resolution (Δx)

Figure 3 shows that the encounter rate is higher for the simulations with coarse grid resolution. After approximately 23 minutes all the particles close to the lower benthic layer are extracted and few new particles are brought down within reach for the corals for the simulations with coarse grid. This time agrees with the time it will take for a particle to travel through the full domain. For the simulations with finer grid, Figure 3 shows that the bottom benthic layer is not drained for particles the first 23 minutes. This is especially prominent in Exp 7 which is the experiment with highest grid resolution, where the encounter rate increases after 15 minutes. The continuous transport of particles into the bottom benthic layer is due to the development of turbulence in the bottom boundary layer which allows for vertical movements of the water masses, and to model this demands very high spatial resolution.

To compare the results from different horizontal grid resolutions, grid resolutions higher than 3.2 m are summed up at 3.2 m intervals. Figure 4 show this average (over 3.2 m) distribution of the encounters. The figure show that the maximum number of encounters will

be on the leading edge of the reef. With increasing resolution the distribution of the encounters will be flattened. The maximum hit rate for all the simulations are found between 150 and 170 m. This is at the front part of the reef and where the compression rate of the stream lines is highest.

Figure 5 and Figure 6 show the actual location of the encounters relatively to the reef. The results show that there are few encounters in the area close to the top of the reef but there are encounters at the lee side of the reef. However, the number of encounters on the rear of the reef is small compared with the number of encounters at the front.

3.2 Sensitivity to the vertical grid resolution (Δz)

The simulations with increasing vertical grid resolution in the lower 12.8 m show that the results are very sensitive to the vertical grid resolution, see Figure 7. Exp 11 and 12, with 0.8 m and 0.4 m vertical grid resolution, respectively, have a significantly different encounter rate than the other simulations. The reason for this is still not understood, but it shows the importance of resolving the lower layer.

Figure 8 shows that the distribution of the average over 3.2 m will have a maximum at the leading part of the reef. The location of the maximum is further upstream on the reef for increasing vertical resolution. The results from Exp 11 show two pronounced peaks in the location of the encounters. The maximum is located over the steepest part of the slope. There are also some encounters at the rear part of the coral reef, but the number of encounters are small.

Figure 9 and Figure 10 show that it is the leading part of the coral reef that will have the highest number of encounters. With increasing resolution the maximum location of the encounters are moved toward the beginning of the coral reef. There are a few encounters on the top of the reef and on the upper part of the rear of the reef, but these encounters are substantially less then the encounters at the leading part of the reef.

3.3 Sensitivity to viscosity, bottom friction, and hydrostatic approximation

Figure 11 show that the number of encounters are fairly robust to variations in the horizontal viscosity. For the vertical eddy viscosity, Figure 15, the variations are larger and high viscosity seems to increase the number of encounters. The distribution of the encounters averaged over 3.2 m show that the maximum of the encounters are found at the leading part of reef, see Figure 12 and Figure 16. The location of the maximum peak varies with changes in the vertical eddy viscosity. High values will lead to increased numbers of encounters up slope for the vertical eddy viscosity.

Figure 13, Figure 14 and Table 1 show that variations in the horizontal viscosity does not significantly change the location of the maximum encounter peak or the start and end location of the encounter distributions.

The distribution of the encounters becomes more asymmetrical with the maximum at the leading edge of the slope when the vertical eddy viscosity decreases, see Figure 17 and Figure 18

When turning off the bottom friction, there will be a free slip condition and no log layer at the bottom. Figure 20 a) show the maximum and distribution of the encounters at the leading edge of the reef. The distribution is very similar to the other simulations, so it seems as the bottom friction does not affect the distribution much except when the resolution is high enough for turbulence to develop in the bottom boundary layer. Figure 20 b) shows the encounter distribution when the lower benthic layer is in the vertical and not perpendicular on the bottom. There is no significant variations in the results compared with Exp 4. Figure 20 c) shows the distribution when the model is run hydrostatic and it is seen that the hydrostatic approximation does not change the particle distribution for this resolution. Compare with Exp 4 which has an identical setup which is run non-hydrostatic.

4 Discussion

Numerical simulations of particle movement for different horizontal and vertical grid resolutions and viscosities have been performed in 2D (x,z). An idealized coral reef with height 16 m and length 90 m has been chosen as bottom topography for the experiments. The inflowing speed is 0.25 ms^{-1}, which gives a Reynolds number $\sim 10^4 - 10^5$. The Reynolds number is important to determine the character of the flow, since it compare inertial and frictional forces in fluids. Turbulence is very likely to occur when the Reynolds Number is greater then $10^5 - 10^6$ [Pond and Pickard, 1983] but can occur earlier dependent on the shape of the reef. In the model result the flow is laminar, except for extreme high horizontal grid resolutions when the bottom boundary layer becomes turbulent. The particles used in the simulations have neutral buoyancy, and drifts passively with the currents. Particles that enter closer than 0.25 m from the bottom are taken out of the simulations and the location is stored for studying suitable areas for corals.

The results show that the distribution of encounters will be located on the leading side of the reef with a maximum in front of the steepest part of the slope. To the lee side of the reef there are found encounters but the number are small compared with the leading part of the reef. This means that if the current is the main factor for bringing food to the corals there will be no preferred growth direction when the current direction changes often, and symmetrical or round reefs will probably be formed. If the current direction is very stable over time, there will be a preferred growth direction facing the current, and elongated reefs with a living head and a dead tail will be formed. This is supported from observations where elongated reefs are found where the current direction is relatively stable and circular reefs is more common where the current direction varies.

The flow of water will generate a horizontal divergence where variations in the bottom topography are present, and therefore create vertical flow. The vertical flow will be upward when the horizontal flow increases in speed when entering shallow areas, and negative then the horizontal flow reduces in deeper areas. The vertical flow is strongest over the steepest parts of the reef. This horizontal divergence is an important factor for the transportation of particles down towards the seabed or in from the surroundings, where benthic organisms can catch them.

The results show that the highest number of encounters occurred in front of the steepest slope. It can be seen that the pathlines of the particles will be closest to the benthic layer when undergoing flow over uneven topography. This means that more particles enter within reaching distance for the corals when flowing over a reef. However, particles that are not caught by the front part of the reef will be close to the reef all the way to the top of the reef, which means that even though the simulations show few encounters there, it still might be a good feeding location for corals.

The numerical results show that the encounter distribution is robust to changes in grid resolution, viscosity, bottom friction, and the hydrostatic approximation. However, there are some vertical grid resolutions that give anomalies in the location of the maximum and the number of encounters compared to the mean and this is still not understood. A horizontal grid resolution of 0.2 m or higher will be able to resolve the turbulence from the bottom boundary layer. This turbulence lead to vertical movements along the bottom in the full domain allowing for particle transport close to the bottom not only in the vicinity of the idealized reef.

There are several important forces that can drive horizontal flow at the Norwegian shelf. The Norwegian Atlantic Current dominates the flow along the continental shelf edge outside Norway, see Orvik et al. [2001] and Orvik and Skagseth [2003]. This inflow will set up an Ekman transport in the lower layer, causing vertical exchanges of water and matter and cross shelf movements of the surrounding water masses. Atmospheric low pressures are frequently passing Norwegian waters. They can force flow by water level rise, however, more interesting is that the wind can cause up or down welling events along the coast and therefore flow in the deeper layer. The Norwegian Coastal Current flow north along

Exp	Δx	IM	min(Δz)	KB	H-Visc	H-Visc2d	V-Visc	#	Max loc
1	6.4	64	0.09	101	0.0	0.0	10^{-9}	2027	160.0
2	3.2	126	0.09	101	0.0	0.0	10^{-9}	1043	160.0
3	1.6	250	0.09	101	0.0	0.0	10^{-9}	551	158.4
4	0.8	498	0.09	101	0.0	0.0	10^{-9}	331	160.8
5	0.4	994	0.09	101	0.0	0.0	10^{-9}	218	158.8
6	0.2	1986	0.09	101	0.0	0.0	10^{-9}	184	161.6, 166.4, 168.8 (165.6)
7	0.1	3970	0.09	101	0.0	0.0	10^{-9}	271	163.7, 179.3 (171.5)
8	0.8	498	6.4	27	0.0	0.0	10^{-9}	302	168.0
9	0.8	498	3.2	27	0.0	0.0	10^{-9}	239	168.8
10	0.8	498	1.6	54	0.0	0.0	10^{-9}	247	165.6
11	0.8	498	0.8	107	0.0	0.0	10^{-9}	1242	173.6
12	0.8	498	0.4	213	0.0	0.0	10^{-9}	871	162.4
13	0.8	498	0.2	251	0.0	0.0	10^{-9}	441	156.0
14	0.8	498	0.1	301	0.0	0.0	10^{-9}	318	159.2
15	0.8	498	0.09	101	2.5E-01	5.0E+00	10^{-9}	303	164.0
16	0.8	498	0.09	101	2.5E-02	5.0E-01	10^{-9}	298	157.6, 166.4 (162.0)
17	0.8	498	0.09	101	2.5E-03	5.0E-02	10^{-9}	313	168.0
18	0.8	498	0.09	101	2.5E-04	5.0E-03	10^{-9}	291	156.0
19	0.8	498	0.09	101	2.5E-05	5.0E-04	10^{-9}	298	164.8
20	0.8	498	0.09	101	2.5E-06	5.0E-05	10^{-9}	310	162.4
21	0.8	498	0.09	101	0.0	0.0	10^{-3}	381	161.6
22	0.8	498	0.09	101	0.0	0.0	10^{-4}	435	161.6
23	0.8	498	0.09	101	0.0	0.0	10^{-5}	338	159.2
24	0.8	498	0.09	101	0.0	0.0	10^{-6}	278	160.8
25	0.8	498	0.09	101	0.0	0.0	10^{-7}	245	158.4
26	0.8	498	0.09	101	0.0	0.0	10^{-8}	319	165.6
27^{*}	0.8	498	0.09	101	0.0	0.0	10^{-9}	301	154.4
28^{**}	0.8	498	0.09	101	0.0	10^{-9}	0.0	310	157.6
29^{***}	0.8	498	0.09	101	0.0	0.0	10^{-9}	356	162.4

Table 1: Exp is the experiment number, Δx is the horizontal grid resolution [m], IM the number of grid cells in the horizontal, min(Δz) is the minimum grid resolution in the vertical [m], KB the number of grid cells in the vertical, Visc and Visc2d the viscosity for 3D and 2D respectively [$m^2 s^{-1}$], # the number of particles that have been taken out during the simulation, and Max loc is the location [m] where most particles have entered the lower 0.25 m (number in parenthesis is the mean if several maximum is found). The experiment marked with *, ** and *** are as Exp 4 run without bottom friction, not including perpendicular catching of particles, and hydrostatic, respectively.

the Norwegian coast will set up currents that can be important for the coral reefs on the continental shelf or at banks. Closer to the coast, tidal effects are important, and in fjords the tide is maybe the most important factor for good feeding conditions on fjord sills. The Norwegian Atlantic Current and the Norwegian Coastal Current are relative stable over time, and can be important factors for the generation of elongated coral reefs.

The results also show that the resolution needed for this kind of experiments will depend on the reef and if the turbulence due to the bottom shear need to be resolved. If the turbulence close to the bottom is of minor importance the horizontal grid resolution should be high enough to resolve the feature of the reef.

Acknowledgement

This research has received support from The Research Council of Norway through NFR 146526/420: Cordino.

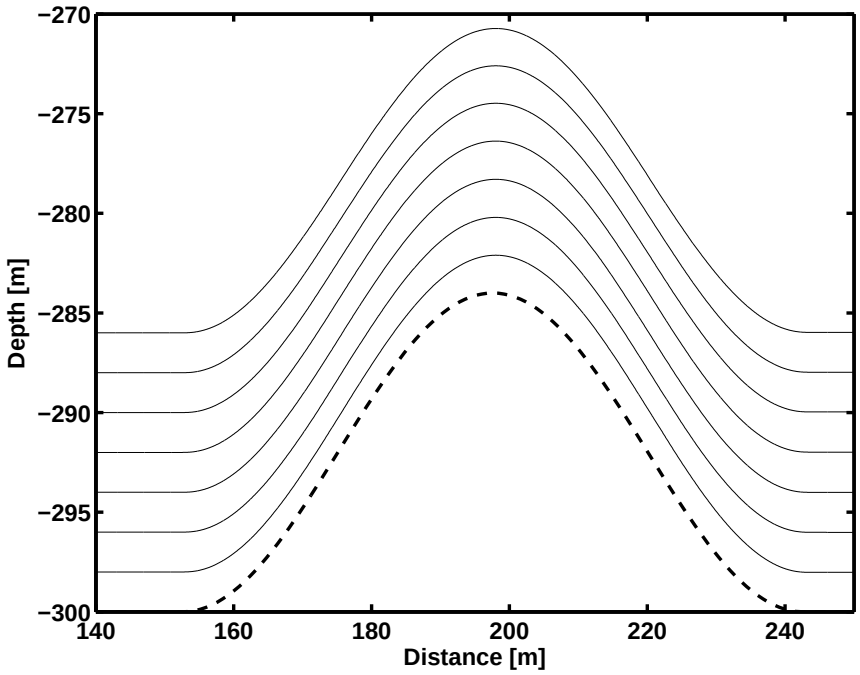

Figure 1: Pathlines of particles that flow over a ridge (Exp 4). The thick black dotted line is the coral reef.

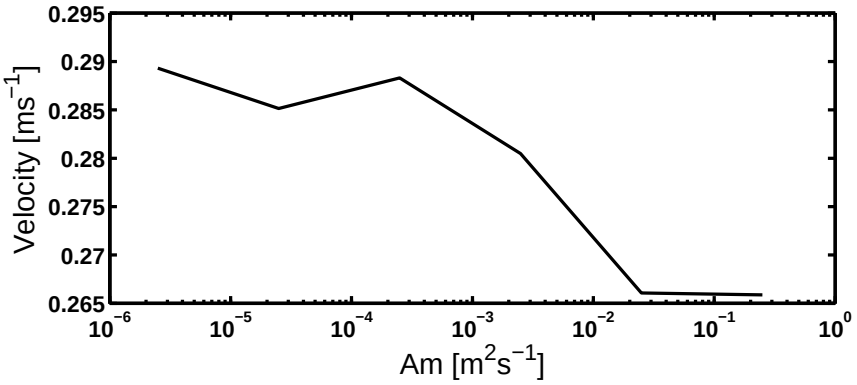

Figure 2: Maximum velocity as a function of the three dimensional viscosity.

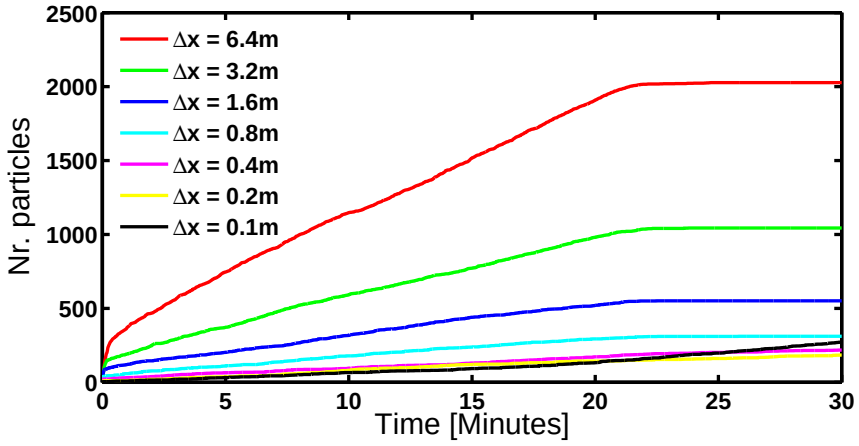

Figure 3: Number of particles that are taken out during the simulation for different horizontal grid resolutions.

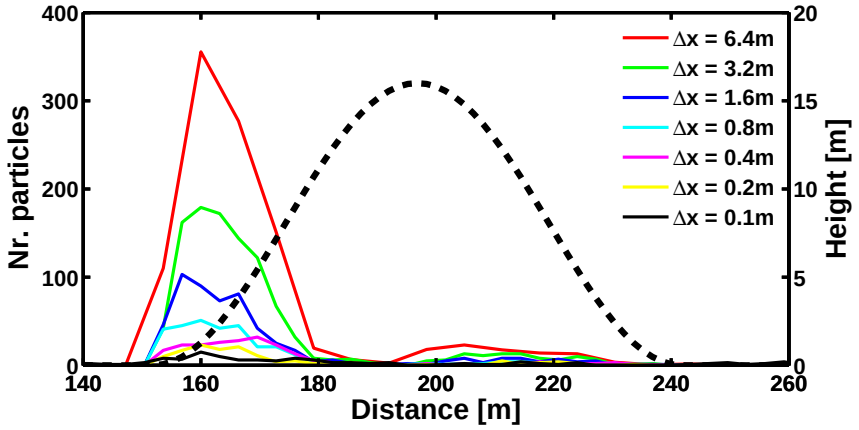

Figure 4: Number and location of where particles have entered the layer 0.25 m above the seabed for the different horizontal grid resolution. The number of particles is summed over intervals of 3.2 m for comparison reasons. The black dashed line is the coral reef with height given on the secondary axis to the right.

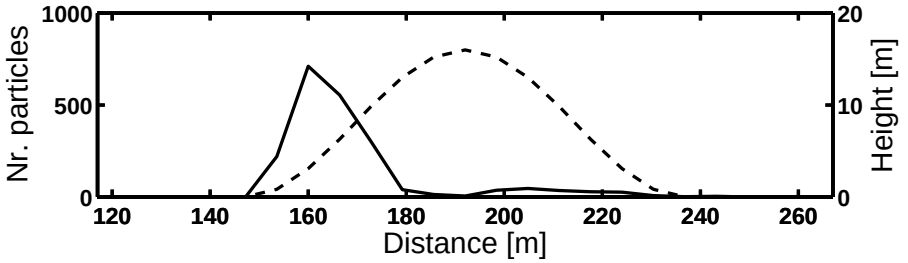

(a) $\Delta x = 6.4\,\mathrm{m}$

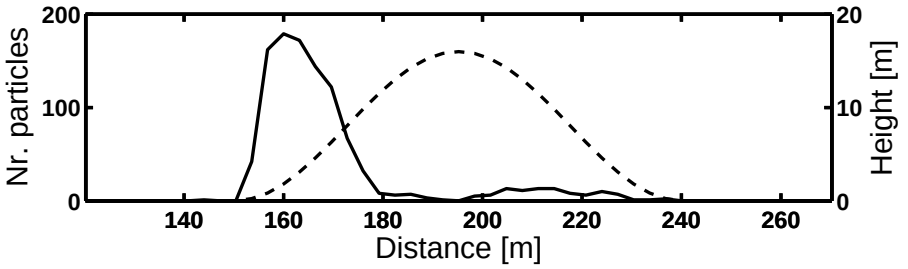

(b) $\Delta x = 3.2\,\mathrm{m}$

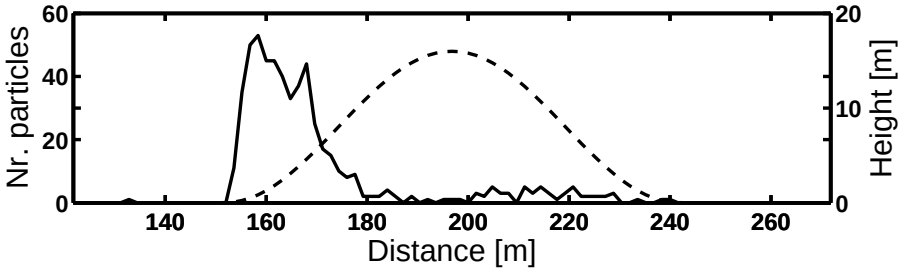

(c) $\Delta x = 1.6\,\mathrm{m}$

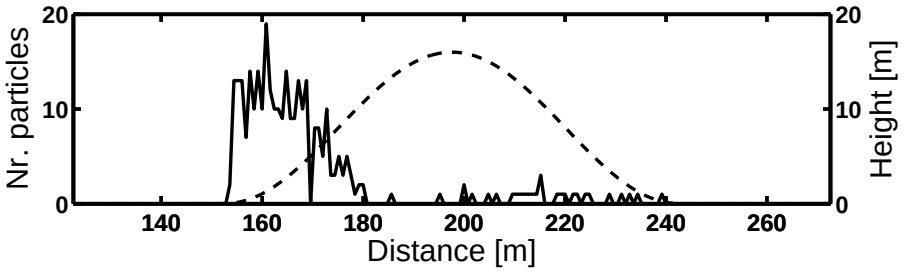

(d) $\Delta x = 0.8\,\mathrm{m}$

Figure 5: Number and location of where particles have entered the layer 0.25 m above the seabed for increasing horizontal grid resolution. The black dashed line is the coral reef with height given on the secondary axis to the right.

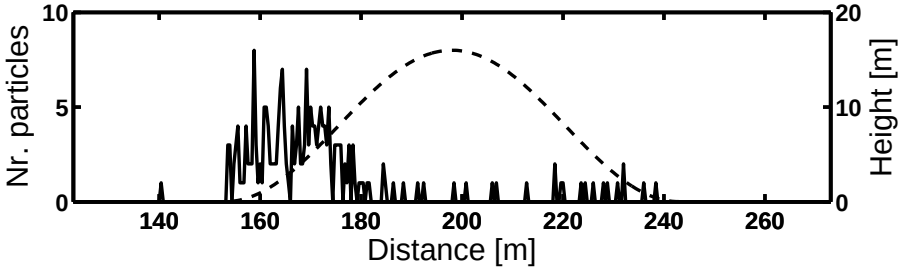

(a) $\Delta x = 0.4\,\mathrm{m}$

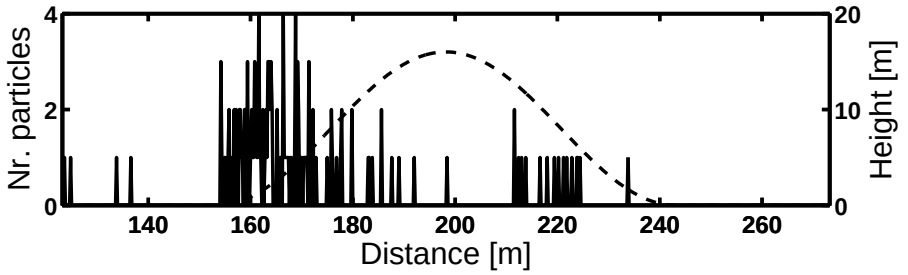

(b) $\Delta x = 0.2\,\mathrm{m}$

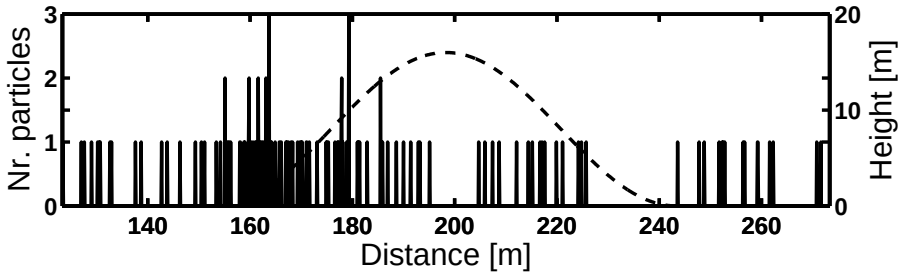

(c) $\Delta x = 0.1\,\mathrm{m}$

Figure 6: Number and location of where particles have entered the layer 0.25 m above the seabed for increasing horizontal grid resolution. The black dashed line is the coral reef with height given on the secondary axis to the right.

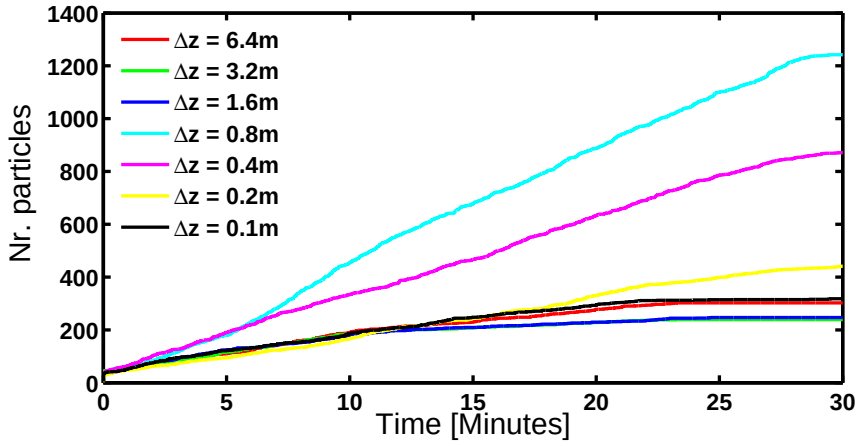

Figure 7: Number of particles that are taken out during the simulation for increasing vertical grid resolutions.

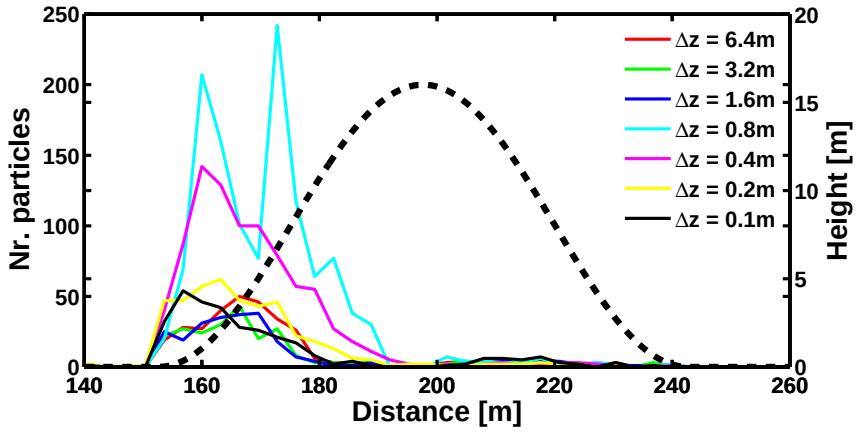

Figure 8: Number and location of where particles have entered the layer 0.25 m above the seabed for the different vertical grid resolutions. The number of particles is summed over intervals of 3.2 m for comparison reasons. The black dashed line is the coral reef with height given on the secondary axis to the right.

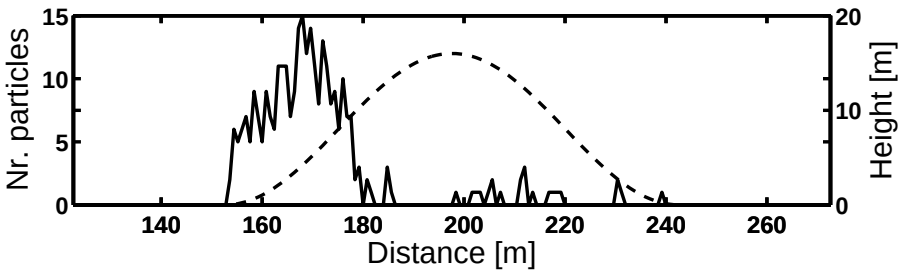

(a) $\Delta z = 6.4\,\mathrm{m}$

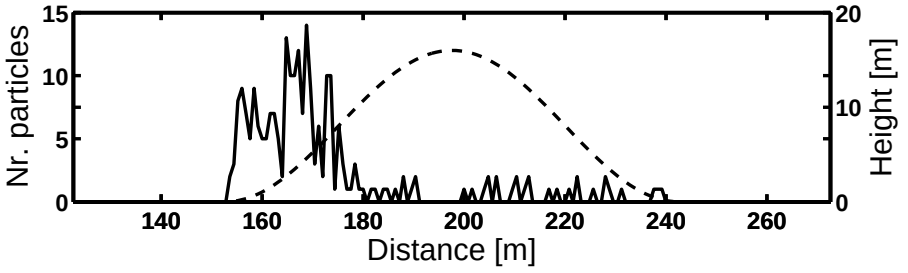

(b) $\Delta z = 3.2\,\mathrm{m}$

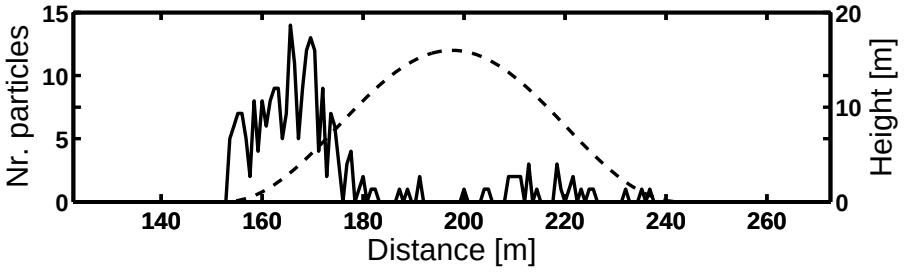

(c) $\Delta z = 1.6\,\mathrm{m}$

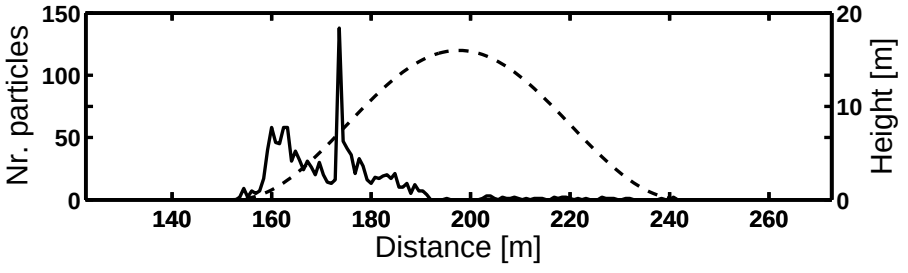

(d) $\Delta z = 0.8\,\mathrm{m}$

Figure 9: Number and location of where particles have entered the layer 0.25 m above the seabed for increasing near seabed vertical grid resolutions. The black dashed line is the coral reef with height given on the secondary axis to the right.

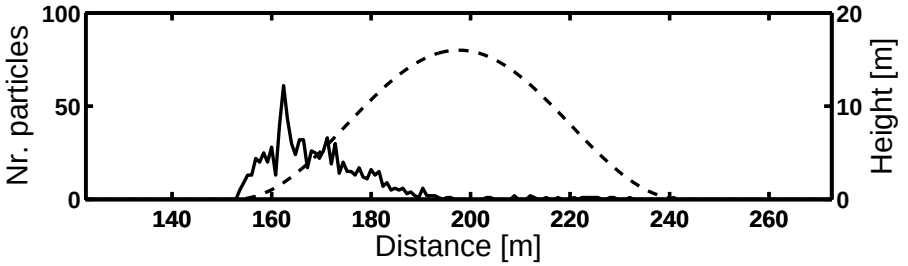

(a) $\Delta z = 0.4\,\mathrm{m}$

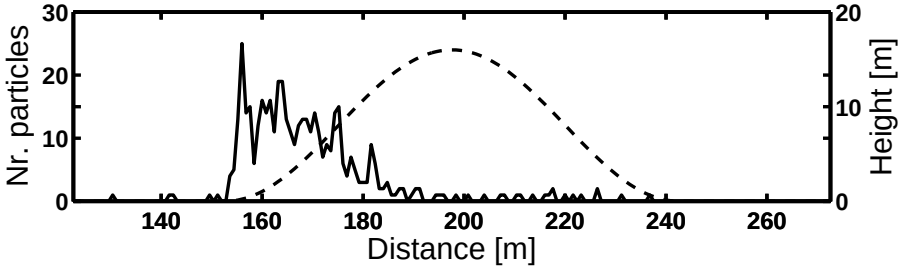

(b) $\Delta z = 0.2\,\mathrm{m}$

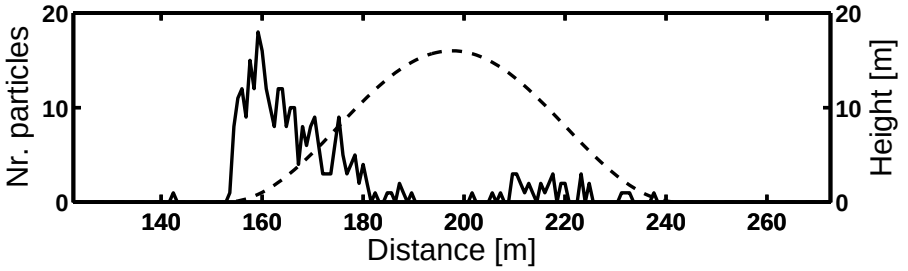

(c) $\Delta z = 0.1\,\mathrm{m}$

Figure 10: Number and location of where particles have entered the layer 0.25 m above the seabed for increasing near seabed vertical grid resolutions. The black dashed line is the coral reef with height given on the secondary axis to the right.

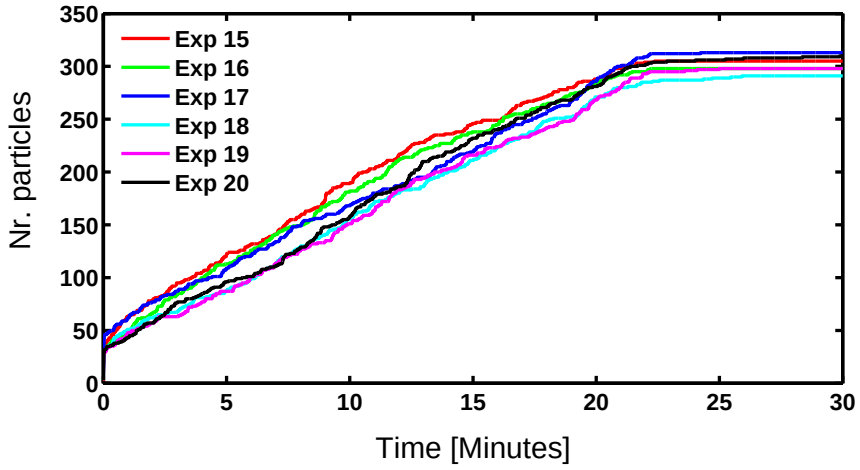

Figure 11: Number of particles that is taken out during the simulation for decreasing horizontal viscosities.

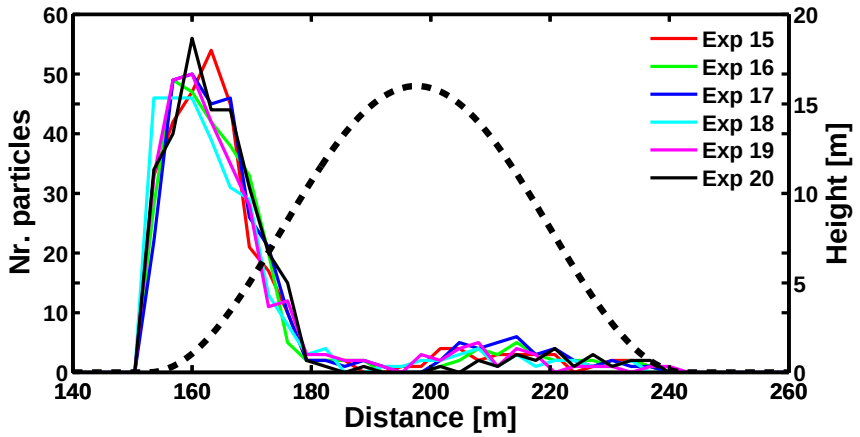

Figure 12: Number and location of where particles have entered the layer 0.25 m above the seabed for decreasing viscosities, see Table 1. The number of particles is summed over intervals of 3.2 m for comparison reasons. The black dashed line is the coral reef with height given on the secondary axis to the right.

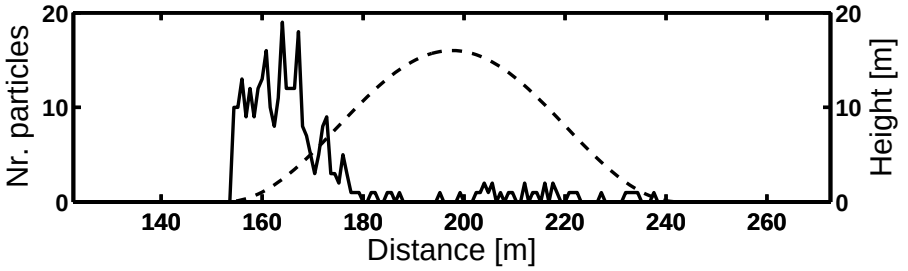

(a) $2.5 \cdot 10^{-1}$ (3D) and 5.0 (2D)

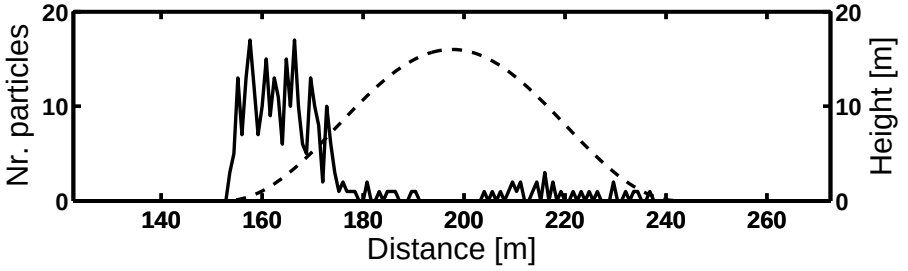

(b) $2.5 \cdot 10^{-2}$ (3D) and $5.0 \cdot 10^{-1}$ (2D)

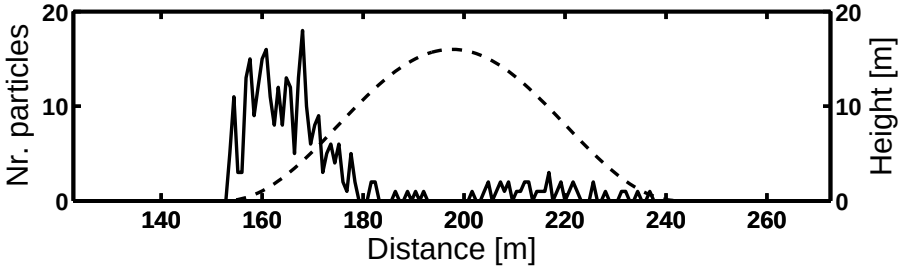

(c) $2.5 \cdot 10^{-3}$ (3D) and $5.0 \cdot 10^{-2}$ (2D)

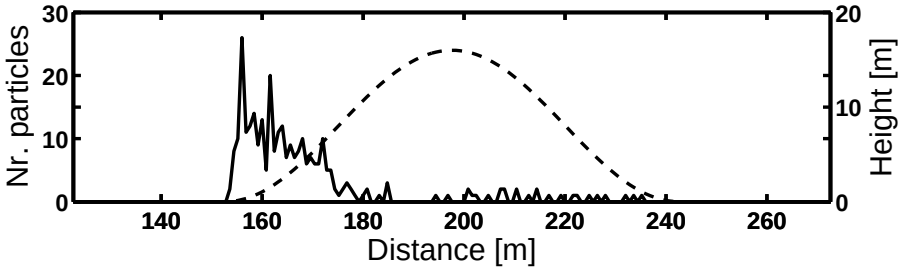

(d) $2.5 \cdot 10^{-4}$ (3D) and $5.0 \cdot 10^{-3}$ (2D)

Figure 13: Number and location of where particles have entered the layer 0.25 m above the seabed for different viscosities (m^2s^{-1}). The black dashed line is the coral reef with height given on the secondary axis to the right. The 3D and 2D viscosities are given as labels in the figure.

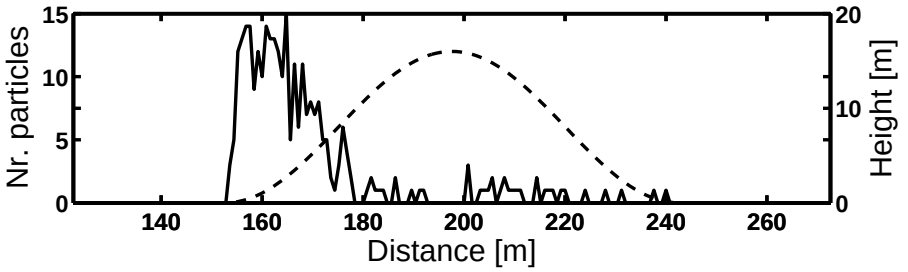

(a) $2.5 \cdot 10^{-5}$ (3D) and $5.0 \cdot 10^{-4}$ (2D)

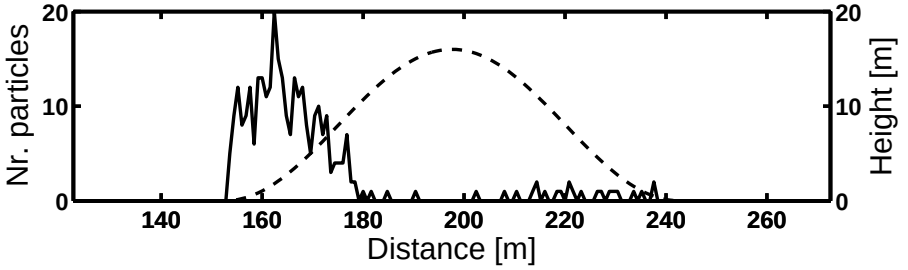

(b) $2.5 \cdot 10^{-6}$ (3D) and $5.0 \cdot 10^{-5}$ (2D)

Figure 14: Number and location of where particles have entered the layer 0.25 m above the seabed for different viscosity (m^2s^{-1}). The black dashed line is the coral reef with height given on the secondary axis to the right. The 3D and 2D viscosities are given as labels in the figure.

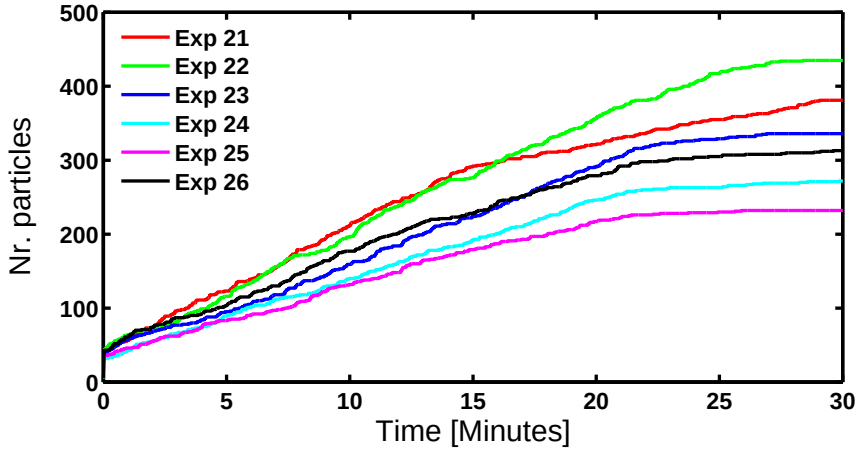

Figure 15: Number of particles that is taken out during the simulation for decreasing vertical eddy viscosity.

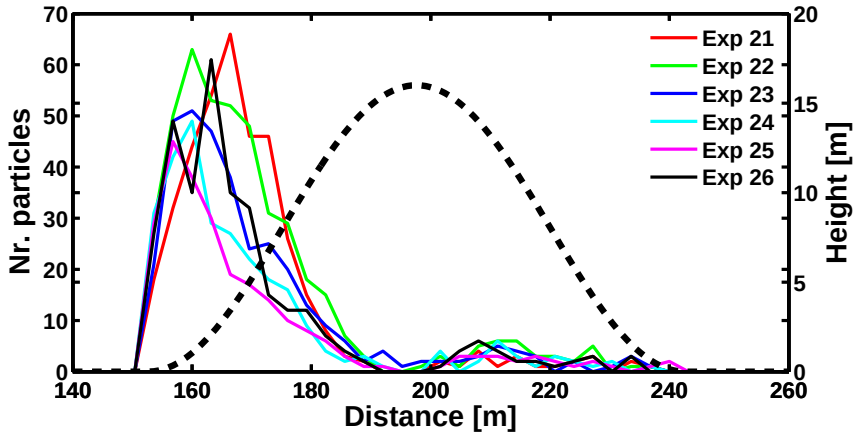

Figure 16: Number and location of where particles have entered the layer 0.25 m above the seabed for decreasing vertical eddy viscosities, see Table 1. The number of particles is summed over intervals of 3.2 m for comparison reasons. The black dashed line is the coral reef with height given on the secondary axis to the right.

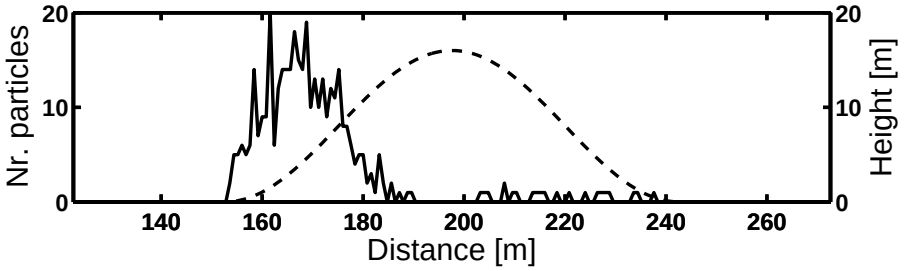

(a) $1.0 \cdot 10^{-3}$

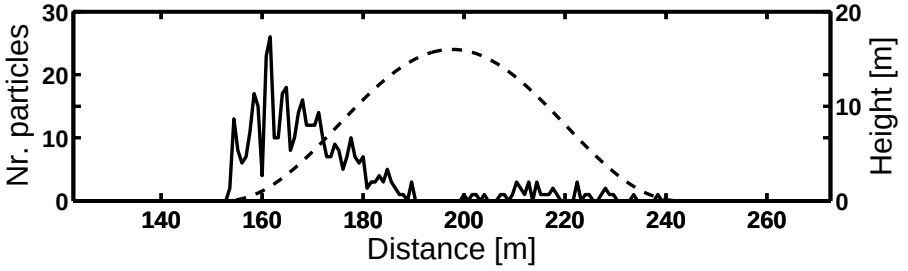

(b) $1.0 \cdot 10^{-4}$

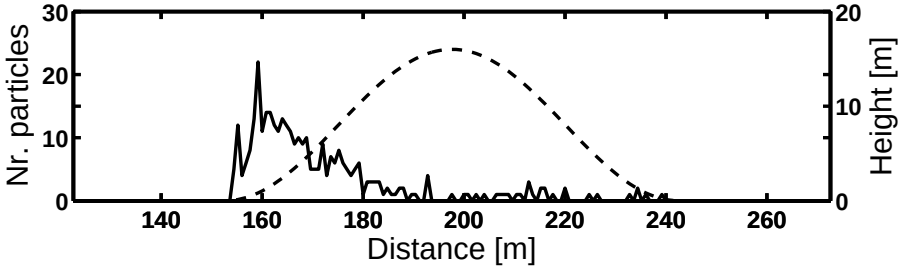

(c) $1.0 \cdot 10^{-5}$

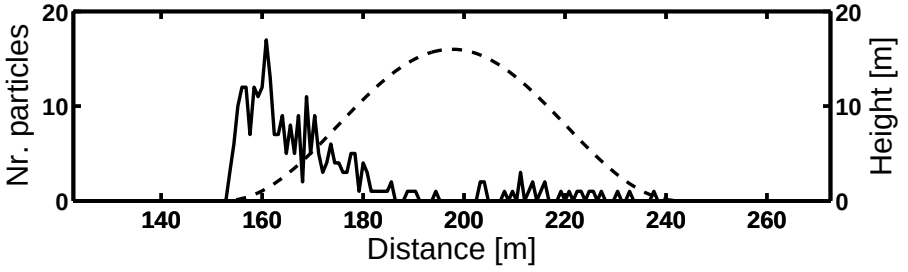

(d) $1.0 \cdot 10^{-6}$

Figure 17: Number and location of where particles have entered the layer 0.25 m above the seabed for different vertical eddy viscosities (m^2s^{-1}). The black dashed line is the coral reef with height given on the secondary axis to the right. The viscosities are given as labels in the figure.

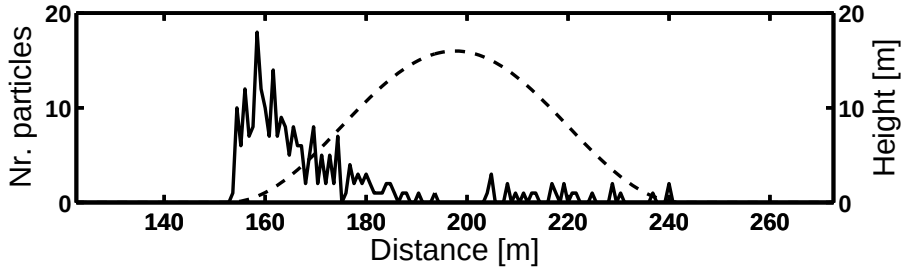

(a) $1.0 \cdot 10^{-7}$

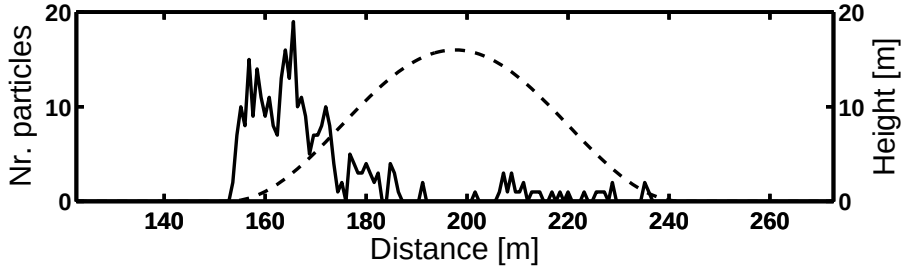

(b) $1.0 \cdot 10^{-8}$

Figure 18: Number and location of where particles have entered the layer 0.25 m above the seabed for different vertical eddy viscosity (m^2s^{-1}). The black dashed line is the coral reef with height given on the secondary axis to the right. The viscosities are given as labels in the figure.

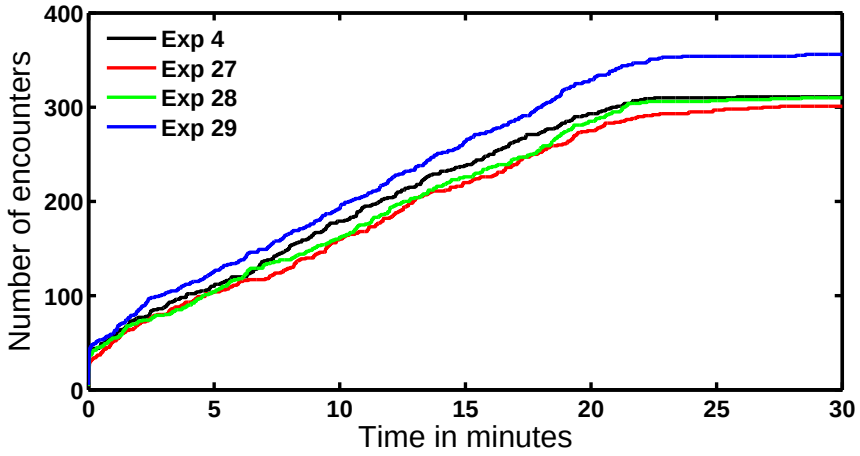

Figure 19: Number of particles that is taken out during the simulation. Red line is the experiment without bottom friction (Exp 27), green line the experiment that does not take into account that the corals can catch particles perpendicular also in areas with varying topography (Exp 28), blue line the experiment that is run hydrostatic (Exp 29), and solid line is Exp 4 which is run with the same parameters but with bottom friction, perpendicular extraction of particles, and non-hydrostatic.

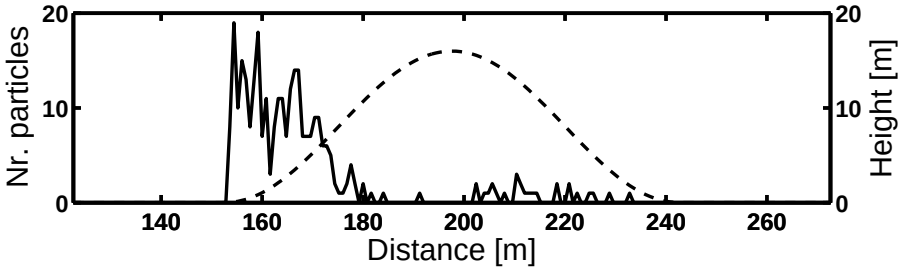

(a) Without bottom friction

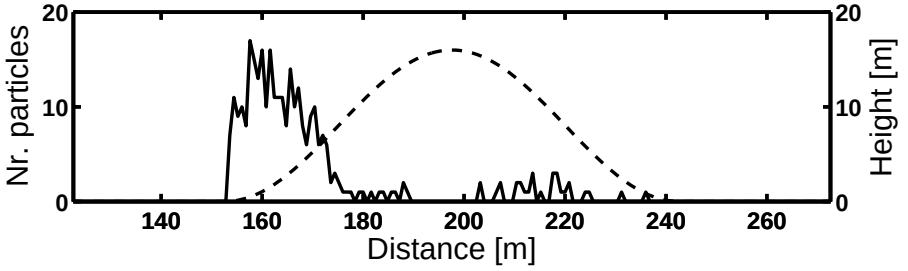

(b) Without perpendicular reach

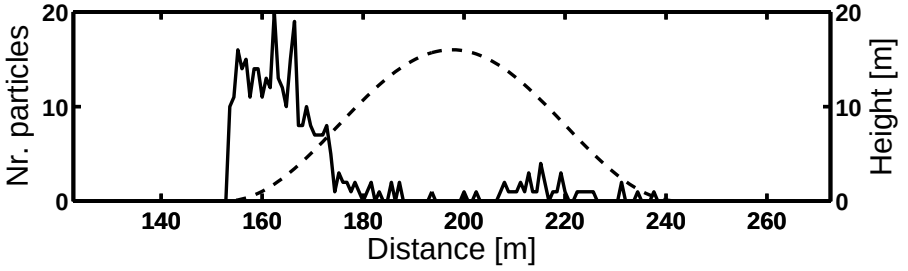

(c) Hydrostatic

Figure 20: Number and location of where particles have entered the layer 0.25 m above the seabed. The black dashed line is the coral reef with height given on the secondary axis to the right.

References

H. Berntsen, Z. Kowalik, S. Sælid, and K. Sørli. Efficient numerical simulation of ocean hydrodynamics by a splitting procedure. *Modeling, Identification and Control*, 2:181–199, 1981. 2.1

J. Berntsen. USERS GUIDE for a modesplit σ-coordinate numerical ocean model. Technical Report 135, Dept. of Applied Mathematics, University of Bergen, Johs. Bruns gt. 12, N-5008 Bergen, Norway, 2000. p. 48. 2.1

J. Berntsen and G. Furnes. Internal pressure errors in sigma-coordinate ocean models-sensitivity of the growth of the flow to the time stepping method and possible non-hydrostatic effects. *Continental Shelf Research*, 25:829–848, 2005. 2.1

A.F. Blumberg and G.L. Mellor. A description of a three-dimensional coastal ocean circulation model. In N.S. Heaps, editor, *Three-Dimensional Coastal Ocean Models*, volume 4 of *Coastal and Estuarine Series*, page 208. American Geophysical Union, 1987. ISBN 0-87590-253-7. 2.1, 2.1

V. Casulli. A semi-implicit finite difference method for non-hydrostatic, free-surface flows. *International Journal for Numerical Methods in Fluids*, 30:425–440, 1999. 2.1

H. Engedahl. Specification of boundary values and use of the flow relaxation scheme in a three-dimensional ocean model. Technical Report 83, Det Norske Meteorologiske Institutt, 1992. 2.2

D.B. Haidvogel and A. Beckmann. *Numerical ocean circulation modeling*, volume 2 of *Series on Environmental Science and Management*. Imperial College Press, 1999. 2.1

Y. Heggelund, F. Vikebø, J. Berntsen, and G. Furnes. Hydrostatic and non-hydrostatic studies of gravitational adjustment over a slope. *Continental Shelf Research*, 24:2133–2148, 2004. 2.1

B.-O. Heimsund and J. Berntsen. On a class of ocean model instabilities that may occur when applying small time steps, implicit methods, and low viscosities. *Ocean Modelling*, 7:135–144, 2004. 2.1

Y. Kanarska and V. Maderich. A non-hydrostatic numerical model for calculating free-surface stratified flows. *Ocean Dynamics*, 53:176–185, DOI 10.1007/s10236–003–0039–6, 2003. 2.1

Z. Kowalik and T.S. Murty. *Numerical Modeling of Ocean Dynamics*, volume 5 of *Advanced Series on Ocean Engineering*. World Scientific, 1993. 2.1

P.K. Kundu and I.M. Cohen. *Fluid mechanics*. Academic Press, 2 edition, 1990. 3

G.L. Mellor. Users guide for a three-dimensional, primitive equation, numerical ocean model. Technical report, Princeton University, 1996. 2004 Version. 2.1

K.A. Orvik and Ø. Skagseth. The impact of the wind stress curl in the north atlantic on the atlantic inflow to the norwegian sea toward the arctic. *Geophysical Research Letters*, 30 (17):1884, 2003. doi: doi:10.1029/2003GL017932. 4

K.A. Orvik, Ø. Skagseth, and M. Mork. Atlantic inflow to the Nordic Seas: current structure and volume fluxes from moored current meters, VM-ADCP and SeaSoar-CTD observations, 1995-1999. *Deep-Sea Research I*, 48(4):937–957, 2001. 4

S. Pond and G.L. Pickard. *Introductory Dynamic Oceanography*. Pergamon Press, 1983. 4

H.Q. Yang and A.J. Przekwas. A comparative study of advanced shock-capturing schemes applied to Burgers equation. *Journal of Computational Physics*, 102:139–159, 1992. 2.1